Spatiotemporal variability of submicrometer particle number size distributions in an air quality management district

Li-Hao Young[a,*], Yi-Ting Wang[a], Hung-Chieh Hsu[a], Ching-Hui Lin[a], Yi-Jyun Liou[a], Ying-Chung Lai[a], Yun-Hua Lin[a], Wei-Lun Chang[a], Hung-Lung Chiang[b], Man-Ting Cheng[c]

[a] Department of Occupational Safety and Health, China Medical University, 91, Hsueh-Shih Road, Taichung 40402, Taiwan

[b] Department of Health Risk Management, China Medical University, 91, Hsueh-Shih Road, Taichung 40402, Taiwan

[c] Department of Environmental Engineering, National Chung Hsing University, 250, Kuo-Kuang Road, Taichung 40254, Taiwan

*Corresponding author: Tel.: +886-4-2205-3366 Ext.6219; Fax.: +886-4-2207-5711; Email: lhy@mail.cmu.edu.tw

Abstract

First measurements of ambient 10-1000 nm particle number concentrations (N_{TOT}) and size distributions were made at an urban, coastal, mountain and downwind site within the Central Taiwan Air Quality Management District during a cold and a warm period. The primary objectives were to characterize the spatial and temporal variability of the size-fractionated submicrometer particles and their relationships with copollutants and meteorological parameters. The results show that the ultrafine particles (<100 nm) are the major contributor to the N_{TOT}. The mean N_{TOT} was highest at the urban site, whereas lower and comparable at the three other sites. Although the mean N_{TOT} at each site showed insignificant differences between study periods, their diurnal patterns and size distribution modal characteristics were modestly to substantially different between study sites. Correlation analyses of time-resolved collocated aerosol, copollutants and meteorological data suggest that the observed variability is largely attributable to the local traffic and to a lesser extent photochemistry and SO_2 possibly from combustion sources or regional transport. Despite sharing a common traffic source, the ultrafine particles were poorly correlated with the accumulation particles (100-1000 nm), between which the latter showed strong positive correlation with the $PM_{2.5}$ and PM_{10}. Overall, the N_{TOT} and size distributions show modest spatial heterogeneity and strong diurnal variability. In addition, the ultrafine particles have variable sources or meteorology-dependent formation processes within the study area. The results imply that single-site measurements of $PM_{2.5}$, PM_{10} or N_{TOT} alone and without discriminating particle sizes would be inadequate for exposure and impact assessment of submicrometer particle numbers in a region of diverse environments.

Keywords: nanoparticles, number size distribution, spatial distribution, temporal variability, exposure assessment, emission sources

1. Introduction

Atmospheric particles have significant implications in climate, environmental and human health. These microscopic airborne particles, on a global scale, influence climate by absorbing and scattering solar radiation, modifying cloud formation, lifetime and precipitation (Rosenfeld et al., 2008). On a regional scale, they degrade air quality and impair visibility (US EPA, 2010a). On a microscopic scale, elevated particle concentrations play a major role in exerting adverse human health effects (US EPA, 2010b). The extent of those effects depends on the particle size, concentration and chemical composition (e.g., Dusek et al., 2006; Zanobetti and Schwartz, 2009; Peng et al., 2009). Studies have shown smaller particles are more pertinent to adverse human health effects, thereby resulting in a worldwide regulatory focus shift from TSP to PM_{10}, and then to $PM_{2.5}$. More recently, ultrafine particles (UFP, < 100 nm) are attracting growing concerns due to their potential higher toxicity and ability to deposit efficiently in the alveolar region upon inhalation (Nel et al., 2006).

Numerous studies have implicated primary vehicle emissions and secondary new particle formation (NPF) as the two major sources of UFP. A comprehensive review paper of ambient UFP from the two sources has been given by Morawska et al. (2008). In addition to sources, meteorological and environmental factors such as wind speed,

temperature, relative humidity, mixing height, local-scale roadside structures, interactions of multiple streets and topography also could play an important role in modulating the spatial and temporal variability of particle number size distributions (Zhu et al., 2002; Wehner and Wiedensohler, 2003; Zhu et al., 2004; Paatero et al., 2005; Hussein et al., 2006; Bowker et al., 2007; Ogulei et al., 2007; Jamriska et al., 2008; Wang et al., 2011a; Wang et al., 2011b; Sabaliauskas et al., 2011).

Strong temporal variability of particle number has been widely reported, especially for the UFP as compared to the accumulation particles (e.g., Wehner and Wiedensohler, 2003; Wang et al., 2011b). In urban environments, the diurnal pattern of particle number is typically characterized by a peak concentration in the morning and another in the early or late evening (Jeong et al., 2004; Park et al., 2008; Lonati et al., 2011; Wang et al., 2011b). The former is particular distinct in traffic-impacted areas, whereas the latter is less consistent due to the variable sources and meteorological conditions in different areas. In addition, a third peak concentration due to NPF event could occur around midday or in the early afternoon. This is the time of day when photochemistry is most intense and the increase of mixing height lowers the pre-existing particle concentration (Young and Keeler, 2007; Moore et al., 2007; Park et al., 2008; Wang et al., 2010; Wang et al., 2011b). The threshold of pre-existing particle concentration for NPF is not an

absolute value but a relative term, which additionally needs to take into account of the condensable vapor concentration (e.g., H_2SO_4) (Stanier et al., 2004a; McMurry et al., 2005). For example, Kulmala et al. (2004) have reported that NPF events were observed in all types of environment, i.e., not limited to clean environments but included polluted ones (Zhu et al., 2004; Dunn et al., 2004; Monkkonen et al., 2005; Wu et al., 2007; Yao et al., 2010). On a seasonal basis, a number of studies have shown that the particle number concentrations are lowest in the summer and highest in the winter. In addition, the smallest size fraction (<50 nm) of UFP shows the strongest seasonal fluctuations (Wehner and Wiedensohler, 2003; Jeong et al., 2004; Harrison and Jones, 2005; Wang et al., 2010; Wang et al., 2011b). Poor atmospheric mixing and low temperatures are the two main reasons leading to elevated particle number concentration in the winter.

Spatial variability of particle number concentrations has been commonly studied by taking measurements as a function of distance from the emission source. These studies have shown a continuous decrease of particle number concentrations while the particles advect away from the road (e.g., Zhu et al., 2002; Zhu et al., 2004; Kittelson et al., 2004; Westerdahl et al., 2005; Buonanno et al., 2009). In a downwind buffer zone of no traffic and little obstruction from buildings, Zhu et al. (2002; 2004) showed that the roadway particle number, CO and black carbon decrease exponentially with distance and then

become indistinguishable from the background level at a distance of 300 m. Furthermore, the decrease rate is slower in the winter than in the summer. The resulting changes in the number size distribution during the road-to-ambient process were attributed largely to condensation, evaporation and dilution, and to a lesser extent to coagulation and deposition (Zhang et al., 2004). In a more complex environment of multiple streets, Ogulei et al. (2007) observed much different patterns of source impacts on the particle number size distributions. Using highly time-resolved data, the authors were able to show distinction between fresh versus aged diesel particles and spark- versus compress-ignition engine emissions. Another way to determine spatial variability is to take measurements at several locations within a city or region. However, data from this type of study are still relatively sparse. Harrison and Jones (2005) showed that the particle number concentrations at seven out of eight sites in the UK were generally similar, suggesting little inter-urban variability in the urban air. One-year concurrent measurements of particle number at five different sites in the Los Angeles Basin showed low to modest spatial correlations for particle number (Sardar et al., 2004). Moore et al. (2009) found the intra-community variability of UFP concentrations at 14 sites in urban Los Angeles is comparable to and exceeds the inter-community variability presented in earlier studies. In the same study, the concentration variability of smaller particles (< 40 nm) was found to

be higher than larger particles (Krudysz et al., 2009). A follow-up study by Hudda et al. (2010), with additional measurements at receptor sites up to 115 km downwind to Los Angeles, also suggested that the intra-community variability was larger than the inter-community variability. More recently, Wang et al. (2011b) showed that, despite uniform temporal variation, the UFP present moderate spatial divergence in urban Rochester, New York. The abovementioned spatial variability has been the largest uncertainty in exposure estimates for population-based epidemiological studies (US EPA, 2010b).

Earlier studies of UFP in Taiwan have focused primarily on particle mass and chemical composition (e.g., Lin et al., 2005; Hsieh et al., 2009; Chen et al., 2010a). Measurements of ambient submicrometer or UFP number size distributions are lacking until recent years (Chang and Lee, 2007; Chen et al., 2010b; Cheng et al., 2010a; Cheng et al., 2010b; Chen et al., 2011). Despite these progresses, the spatial and temporal variability of particle number size distributions has yet been addressed. With that in mind, the present study selected four sampling sites in the Central Taiwan Air Quality Management District (CTAQMD) for characterizing the spatiotemporal variability of submicrometer particle number size distributions and their relationships with copollutants and meteorological parameters. The selected sites encompass relatively diverse environments, including an urban, coastal, mountain and downwind area. Measurements

were carried out consecutively among the sites during a cold and a warm period. In addition to complementing earlier studies, the results of the present study will serve as the foundation for future in-depth particle number size distribution studies. The outputs are pertinent to obtaining a more representative assessment of their impact on human and environmental health.

2. Material and Methods

2.1 Sampling Sites

The aerosol sampling campaigns took place in the CTAQMD, one of the seven air quality management districts designated by the Taiwan Environmental Protection Administration (TW EPA) (http://www.epa.gov.tw/). The CTAQMD includes the Greater Taichung City, Nantou County and Changhua County, and covers an area of ~ 7,400 km^2 with a registered population of ~4,480,000. It is to be noted that the registered number of vehicles is approximately the same as the registered population. The highest population density of ~ 6570 inhabitant km^{-2} is in the Taichung urban area, whereas the lowest of ~ 130 inhabitant km^{-2} in Nantou County.

Four out of the 12 TW EPA air quality monitoring sites in the CTAQMD were selected to nominally represent urban, coastal, mountain, and downwind areas. They

include Jhongming (JM), Siansi (SS), Puli (PL), and Jushan (JS) site, respectively. The sites are 20-50 km apart as shown in Figure 1 and the site-specific information is given in Table 1. The JM site is located in the center of the Taichung urban basin. This site is 15 m above ground level (AGL) and within 150 m to a major, high-traffic crossroad of width 35 m. There are a total of ~ 2,610,000 registered vehicles in the Taichung City, ranking 3rd in the country (TW Ministry of Transportation and Communications, http://www.motc.gov.tw/). Among these vehicles, 65% are 4-stroke and 2-stroke scooters (ratio=7:3), 30% are mostly gasoline-powered passenger cars, and the remaining 5% are trucks, buses and other types of vehicles. The SS site is situated 4.8 km to the western coastline of Taiwan, 10 km to the east of a major industrial park, 9 km south to the largest coal-fired power plant in Taiwan. This site is 13 m AGL and 150-m away from a low-traffic road of width 23 m. The PL site is positioned in a relatively rural basin inside the mountainous regions, where to its east is the Central Mountain Ranges of height 2-3 km. An east-west direction corridor is the only major route that connects this area to the rest of the Central Taiwan areas. The PL site has an elevation of 454-m above the mean sea level, and is located 21-m AGL, 25-m away from the nearest major road. The JS site is near the southern border of the CTAQMD, in between hills that stretch in north-south direction, 44 km to the southeast of the Taichung urban area, 8-m AGL and 150-m away

from a major road of width 15 m. The prevailing northeasterly trade winds during winter months are conducive for transport of air pollutants from the Central Taiwan region to the JS site. As a result, the TW EPA had designated it as a photochemistry site.

2.2 Instrumentation

The number size distributions of ambient aerosols were measured by a scanning mobility particle sizer (SMPS; Model 5.500, GRIMM Aerosol Technik, Gmbh, Germany), housed inside the monitoring sites. The sampling set up was nearly identical among all the sites, described in the following. Ambient sample air was drawn through the site rooftop at a flow rate of 8 liters min^{-1} (lpm) with a 3-m glass tube. The tube of 2.5-m was extended vertically outdoor and shielded inside an aluminum tube. A short stainless steel forward-facing probe was inserted into the glass tube to draw a small portion of the sample air into the SMPS through a 1.5-m conductive tubing at 0.3 lpm. The diffusion loss to the glass and conductive sample line was estimated to be ~15% for the smallest measureable particles of 11.1 nm (Baron and Willeke, 2001), though no loss corrections were made to the measured data. The air conditioners inside the sites were activated only when the indoor temperature exceeded 31 °C; therefore, the indoor as well as the sample air temperature basically follows the ambient temperature trend. For example, the highest

daily ambient temperature of 31.5 °C was slightly higher than the sample air temperature inside the differential mobility analyzer (DMA) of 29.5 °C on that same day. Similarly, the lowest daily ambient temperature of 11.8 °C was slightly lower than the sample air temperature inside the DMA of 15.4 °C on that same day. As a result, there were no observed water condensation issues with the sampling tube.

The SMPS consists of a long Vienna-type DMA (L-DMA; Model 55-900) and a butanol-based condensation particle counter (CPC; Model 5.403). The operating principles of the system are described in detail elsewhere (Winklmayr et al., 1990; Reischl et al., 1997; Heim et al., 2004). The inlet of the L-DMA consists of an impactor with a 50% collection efficiency at 1082 nm, followed by an Am-241 neutralizer (Model 5.522). With its default set up, the inner electrode of the L-DMA is positively charged. The detectable aerosol mobility diameters range from 11.1 to 1083.3 nm (44 size bins) with a sheath and sample flow of 3 lpm and 0.3 lpm, respectively. Due to the humid condition in Taiwan, the sheath air is dried to a RH of ~10% through a silica gel canister and then passed through a HEPA filter before entering the L-DMA. The saturator and condenser temperature of the CPC was set at 40 °C and 15 °C, respectively. The CPC has a 50% counting efficiency at 4.5 nm and measures number concentration up to 2×10^4 cm^{-3} with single particle counting and coincidence correction, and up to 10^7 cm^{-3} with the

photometric mode. The SMPS was set to down-scan 6 min and 26 s from 10,000 to 5 V plus a wait-time of 34 s, producing one average particle number size distribution every 7 min. The SMPS has been routinely sent back to the manufacturer for calibration each year. In addition, the sizing accuracy was determined before the study by sampling NaCl of known mobility sizes (50, 76, 113, 168, and 241 nm) from a monodisperse aerosol generator (TSI; Model 3475), simultaneously with another SMPS (TSI; Model 3936). The differences between the expected and the measured mode sizes were less than 3 nm.

On-site air quality and meteorological data were obtained from the monitoring sites and validated by the TW EPA (TW EPA, 2009). At the sites, PM_{10} and $PM_{2.5}$ were continuously monitored by means of β-ray attenuation, SO_2 by UV fluorescence, NO_x by chemiluminescence, CO by nondispersive IR, and O_3 by UV absorption. Meteorological parameters used in this study include T, RH, wind speed and direction.

2.3 Sampling Campaigns

Two intensive sampling campaigns were carried out from October 2008 to January 2009 and August 2010 to October 2010. The site and sampling information are given in Table 1. Based on the overall average temperatures (20.5 vs. 27.6 °C), we conveniently referred to the first and second campaign as the “cold” and “warm” period, respectively

(Table 2). Limited by one SMPS, we continuously measured the aerosol number size distributions for two weeks at each site, and rotated consecutively among the four sites. Between each site, we carried out routine maintenance, including impactor cleaning, system leak tests, zero-tests, and flow rate measurements. During the study periods, we collected a total 26,075 aerosol number size distributions over 137 effective sampling days. The overall data coverage is ~92.5%.

2.4 Data Analysis

The aerosol data were subjected to quality control and assurance procedures described below. First, the data from the largest size bin (1083.3 nm) were discarded to minimize the effect from potential multiple charged particles. Second, following the screening method proposed by Yu et al. (2004), the number concentrations and the relative standard deviations between particle counts of size bins below 100 nm were analyzed to detect potential abnormal size distributions. Only very small numbers of collected aerosol data (<0.1%) were identified as outliers that typically occurred at the beginning of the instrument set up. The outliers were not included in the data analysis. For convenience of discussion, the "total" submicrometer particles hereafter refer to those with sizes between 10 to 1000 nm. Furthermore, the size-fractionated number

concentrations of nucleation (10-25 nm), Aitken (25-100 nm), accumulation (100-1000 nm), and ultrafine (10-100 nm) particles hereafter are denoted as N_{NUC}, N_{AIT}, N_{ACC}, N_{TOT}, and N_{UFP}, respectively. In order to match the time resolution of the air pollutant and meteorological data, the aerosol data were averaged to derive hourly averages of particle number size distributions. The hourly aerosol, air pollutants and meteorological data were then used to compute Pearson product moment correlation coefficients (r) and to determine the temporal variation. In the correlation analysis, each site's datasets for the cold and warm period were combined together to cover more diverse pollutant levels and meteorological conditions as well as increasing the sample size.

The mean particle number size distributions for each site and study period were fitted with three lognormal distributions to identify the underlying sub-modes. The selection of tri-modal fits is because bimodal fits, in a number of cases, failed to account for the accumulation particles. The fitting process was done using the following distribution function (df):

$$\mathrm{df} = \mathrm{A}\exp\left[-\left(\frac{\left(\ln \mathrm{D_p} - \ln \mathrm{D_m}\right)}{\mathrm{W}}\right)^2\right] \quad (1)$$

where A sets the amplitude (peak height), D_m sets the particle mode diameter, and W sets the peak width. The Levenberg-Marquardt algorithm, a nonlinear least-squares fitting, is

used to search for the minimum value of chi-square (χ^2) (Igor Pro v.6.2.2.2, WaveMetrics, Inc.). The square root of the number concentration for each size bin (i.e., the measurement uncertainty of particle counter) was used in the calculation of χ^2 to obtain a more accurate fit as follows:

$$\chi^2 = \sum \left(\frac{y - y_i}{w_i} \right)^2 \quad (2)$$

where y is the fitted value, y_i is the measured value, and w_i is the measurement uncertainty for size bin i. The tri-modal fitting terminates after 40 passes in searching for the best fit, or will quit if 9 passes in a row do not result in a decrease in χ^2.

3. Results and Discussion

3.1 Meteorological Conditions and Air Quality

A detailed description of the typical synoptic weather patterns for each season in Taiwan has been given elsewhere (e.g., Cheng, 2001). The site-specific meteorological conditions during the study are summarized in Table 2. The temporal evolution of the wind speed at each site during the two study periods is presented in Figure S1. With respect to average values, the major differences between the cold and warm period include the ambient temperature (20.6 vs. 27.6 °C), prevailing wind direction (NNW vs. W) and accumulated precipitation (57.4 vs. 283.6 mm). As Taiwan is situated at the

border of the subtropical region, it is important to note that the meteorological differences between seasons are relatively small compared to mid- or high-latitude regions. For example, the minimum and maximum monthly average temperature over the past three decades were 16.6 °C (January) and 28.6 °C (July), respectively, i.e., a range of only 12 °C (Taiwan Central Weather Bureau, http://www.cwb.gov.tw/). Based on these historical data, it shows that the present cold period was warmer (ΔT=4 °C), whereas the warm period is comparable (ΔT=1 °C) to typical conditions.

The site-specific hourly averages and diurnal patterns of air pollutant concentrations are given in Table 3 and Figure S2, respectively. Overall, the major air quality differences between the cold and warm period include the significantly higher PM and NO_x, and slightly higher SO_2 concentration during the cold period. Furthermore, despite the large seasonal and site-to-site differences in PM concentrations, the average percentage of $PM_{2.5}$ over PM_{10} of 65% remained nearly constant.

3.2 Submicrometer Particle Number Concentrations

The summary statistics of the hourly N_{NUC}, N_{AIT}, N_{ACC}, and N_{TOT} and the fraction of N_{UFP}/N_{TOT} during the two study periods are summarized in Table 4. The highest mean N_{TOT} of 3.1×10^4 cm^{-3} and 3.4×10^4 cm^{-3} were measured at the urban site for the cold and

warm period, respectively. These mean N_{TOT} were comparable to that measured at a number of other urban sites, in street canyon and at roadside, but lower than that measured on road and inside tunnels (Stanier et al., 2004b; Harrison and Jones, 2005; Aalto et al., 2005; Moore et al., 2009; Lonati et al., 2011; Bae et al., 2010; Asmi et al., 2011; Wang et al., 2010; Chen et al., 2010a; Cheng et al., 2010a; Cheng et al., 2010b; Wang et al., 2011b; Sabaliauskas et al., 2011). The mean N_{TOT} at the coastal, mountain, and downwind site were similar, in the range of 1.7×10^4-2.2×10^4 cm^{-3}. These averages are 29-49% lower than that measured at the urban site, attributable to the substantially higher N_{UFP} (i.e., N_{NUC}+N_{AIT}) at the urban site. This observation is consistent with earlier studies that showed higher number concentrations at sites impacted by heavy traffic, whereas lower concentrations were distributed more or less homogeneously at background or receptor sites (Harrison and Jones, 2005; Hudda et al., 2010; Bae et al., 2010). Another explanation to the higher N_{UFP} is the frequent NPF events observed at the urban site during the warm period, discussed later in Section 3.3. On the other hand, excluding the storm-impacted downwind site, the lowest mean N_{TOT} of 1.7×10^4-1.8×10^4 cm^{-3} were measured at the mountain site during both the cold and warm periods. The average $PM_{2.5}$ levels (up to 47.7 μg m^{-3}; Table 3) were typically highest at the mountain site. Additionally, its $PM_{2.5}$ and N_{UFP} were negatively correlated (r = -0.25; see Section 3.5).

This suggests a weaker UFP source strength and/or the elevated pre-existing particles are not conducive for the survival of the UFP at the mountain site. Modeling studies have shown that nucleation particles are quickly removed by coagulation with larger background particles or by condensational growth, with time scales of as small as 0.01-0.1 hr (Pandis et al., 1995; Kerminen et al., 2004).

On a daily basis, the mean N_{TOT} on weekdays and weekends were 2.3×10^4 cm^{-3} and 2.2×10^4 cm^{-3}, respectively, with a slightly higher variability during the weekend (Table S1). As shown, the weekday and weekend N_{TOT} differences during the cold and warm period were negligible. Asmi et al. (2011) also have shown no statistically significant variation of concentrations between weekdays and weekends in a number of European sites. On a seasonal basis, the overall mean N_{TOT} at each site during the warm period was generally higher than that during the cold period. The site-specific seasonal differences were < 22 %. This shows that the weekday-to-weekend as well as the cold-to-warm seasonal variability is smaller than the site-to-site spatial variability of N_{TOT}. Unlike the present study, many others have shown a distinct seasonal pattern and weekday-weekday differences in the particle number concentrations, with higher levels observed in colder months and during weekdays (Singh et al., 2006; Aalto et al., 2005; Stanier et al., 2004b; Harrison and Jones, 2005; Moore et al., 2009; Birmili et al., 2010; Bae et al., 2010;

Lonati et al., 2011; Wang et al., 2011a; Sabaliauskas et al., 2011). Paatero et al. (2005) and Sabaliauskas et al. (2011) have shown a negative correlation between particle number and T, where the later covers a range from -4.6 to 28 °C. Marawska et al. (2008) suggested that the seasonal variability is more distinct in mid- and high-latitude regions in the Northern Hemisphere, where the meteorological differences between seasons are significant. For example, no seasonal pattern was identified for the particle number concentration in subtropical Brisbane, Australia (Mejia et al., 2007). Similarly, strong seasonal variability is considered unlikely due to the small temperature difference (~7 °C) between the present two study periods.

Within the submicrometer size range, the percentages of N_{UFP}/N_{TOT} were in the range of 69% to 87%, between which higher values were observed at the urban and coastal site (Table 4). These observations are comparable to that in Milan, Italy (Lonati et al., 2011), but lower than that of 90% in Los Angeles, CA (Moore et al., 2009). The site-to-site as well as the cold-to-warm percent differences of N_{UFP}/N_{TOT} were <17%. Given that the overall mean N_{TOT} of 2.2×10^4 cm^{-3}, the N_{UFP} differences were $<0.4\times10^4$ cm^{-3}. The overall averages and variability of N_{UFP}/N_{TOT} for the cold and warm period were nearly identical. Overall, the N_{NUC}, N_{AIT}, and N_{ACC} were generally similar among the four sites and between the cold and warm period. An exception is the considerably higher N_{NUC} and

N_{AIT} in the range of 1.1×10^4-1.6×10^4 cm^{-3} at the urban site than at the other three sites. This indicates that the urban area is an important source of freshly-formed UFP. On the other hand, the coastal, mountain and downwind site have comparable, relatively weaker UFP source strength, and that their atmospheric conditions (e.g., high PM levels at the mountain and downwind site or strong wind speed at the coastal site) may be unfavorable for the survival of local UFP.

3.3 Submicrometer Particle Number Size Distributions

The temporal evolution of the particle number size distributions measured at the four sites during the cold and warm period is presented in Figure 2. A key feature common to all the sites is that the particle number size distributions show strong diurnal variability during both study periods. The variability is characterized by the active production of UFP during the daytime hours and the disappearance of nucleation particles during the midnight to early morning hours. This indicates that the human activities and photochemistry are the two dominant driving forces behind the emission or production of UFP. Such UFP production is particularly active at the urban site. In specific, we identified frequent NPF events (eight out of 12 days) during the warm period of $PM_{2.5}$ averaging 21.2 μg m^{-3}. Notably, such $PM_{2.5}$ levels are considered “low” in Taiwan (see

Table 3), but not so at urban sites in other countries (e.g., Bae et al., 2010; Wang et al., 2011b). The NPF events are characterized by a burst of the smallest measurable particles of 11.1 nm, followed by continuous particle growth over a period of up to 5 hours. Furthermore, the onset of the urban NPF events was typically before 09 local time (LT), not during midday hours. This suggests the NPF was closely connected to the morning traffic emissions and possibly the breakup of nocturnal inversion layer. Wang et al. (2011a) also reported frequent morning nucleation events in Rochester, NY. However, unlike the present study, those events were not accompanied by particle growth. There were also several NPF events at the other sites, though the frequency and intensity were much lower. At the coastal site, the onset of UFP production and the number size distribution characteristics were more variable than the other sites. At the mountain and downwind site, the onset of UFP production was relatively consistent during the afternoon or midday hours. However, the UFP production was substantially more intense at the downwind site. Details of the NPF and growth events at the four sites will follow in subsequent publication.

The statistical presentations (16th, 50th, 84th percentiles and mean) of the site-specific particle number size distributions are shown in Figures 3 and 4, respectively. Also shown in the figures are the tri-modal lognormal fits to the mean particle number

size distributions. The site-specific size distributions showed considerable temporal variability. In specific, the mean concentrations were typically higher than the 50th percentile concentrations (i.e., skew to the right) for particles in the UFP size range. All the size distributions exhibited two dominant modes, namely the nucleation and Aitken mode, and a minor accumulation mode. Such tri-modality is in agreement with that observed in Milan, Italy (Lonati et al., 2011), but in contrast to the uni-modal median size distributions measured at a number of European sites (Asmi et al., 2011). In this study, the location and intensity (i.e., size and concentration) of the modes show considerable site-to-site and cold-to-warm variability. Nevertheless, three common features are summarized as follows. First, a nucleation mode is always present in the site-specific mean size distributions for the cold and warm period. This indicates the omnipresence of freshly-formed particles. Second, the Aitken and accumulation mode sizes are always smaller during the cold period. This feature may be related to the relatively lower temperature (Table 2), which favors the formation of fresh and smaller particles. Sabaliauskas et al. (2011) observed the geometric mean diameter was smallest during the winter due to increased concentrations of <50 nm particles. Third, the concentrations of the accumulation mode particles are always considerably higher during the cold period. This feature is consistent with the significantly higher PM levels during the cold period

(Table 3). Wang et al. (2011b), however, reported greater accumulation-mode contributions to the total particle numbers in the summer due to regional transport. Overall, the results show that there is notable variability in the particle number size distributions among sites and between study periods, despite having comparable N_{TOT}. This implies that the total particle number concentration alone may not be a representative exposure or impact estimate, both of which depend on particle size.

3.4 Diurnal Variations of Submicrometer Particles

The diurnal variability of the hourly N_{TOT} and air pollutants concentrations at each site is shown in Figures 5 and S2, respectively. During the cold period, the N_{TOT} at the urban, downwind and mountain site showed distinct and consistent diurnal patterns with peak concentrations between 08-09 and 17-19 LT. The peak concentrations ranged from 1.6×10^4 cm^{-3} to 4.4×10^4 cm^{-3}, between which higher values were measured at the urban site and lower ones at the mountain site. Many other studies have shown such a daily two-peak pattern, particularly in the urban area and on workdays (Wehner and Wiedensolher, 2003; Jeong et al., 2004; Hussein et al., 2004; Stanier et al., 2004b; Harrison and Jones, 2005; Birmili et al., 2010). The temporal patterns of CO and NO_x, to a lesser extent for SO_2, correlated well with that of N_{TOT}, especially during the morning

traffic rush hours. This indicates that those particles were predominantly from traffic emissions. Unlike others, the temporal patterns of the size-fractionated particles at the coastal site were quite different from the three other sites. For example, the morning peak concentration at the coastal site was less pronounced and there was no obvious evening peak during the cold period. This is likely due to the considerably higher average wind speeds of 4.3 m s^{-1} near the coast, conducive for atmospheric dispersion. A closer examination of the size-fractionated particle number concentrations reveals that their temporal behaviors are dependent on particle size during the cold period (Figure 6). As shown, the production of nucleation particles was more active in the morning, at noon and in the early evening. The Aitken mode particles were driving the N_{TOT} variability, evident by their nearly identical temporal patterns. The accumulation particles generally followed the temporal patterns of Aitken mode particles, though there is an obvious impact of aged particles at the downwind site. This is likely due to the winter prevailing northerly winds that favors the transport of pollutants from the upwind urban area (Table 2 and Figure 1).

During the warm period, the temporal pattern of N_{TOT} at the four sites was more variable than that during the cold period (Figure 5). The diurnal variability of the hourly N_{NUC}, N_{AIT} and N_{ACC} at each site during the warm period is given in Figure 7. The

mountain site is the only site where the traffic-related two-peak concentration profile of N_{TOT} remained visibly distinct. This is likely because of its unique topography, where the surrounding Central Mountain Ranges are favorable for trapping the air mass that enters through the east-west direction corridor. In the contrary, there were no obvious traffic-related morning N_{TOT} peak concentrations at the urban, coastal and mountain site. In particular, the urban site showed a distinct peak concentration of 6.9×10^4 cm^{-3} at 10 LT. This peak was not only considerably more pronounced but also occurred an hour later than the typical traffic-related morning peak. It was due to the frequent, traffic-related NPF and growth events in the morning, evident by the substantially elevated N_{NUC} and N_{AIT} shown in Figure 7. In comparison, three other intense NPF and growth events were observed only at the downwind site during the warm period. At the coastal and downwind site, the diurnal pattern showed relatively elevated concentrations between 11-15 LT. Compared to the urban site, these daytime peak concentrations were considerably less intense, and they overlapped more during periods of strong solar radiation. This is suggestive of the link between photochemistry and NPF. The more intense and frequent NPF at the urban site is likely a result of its higher traffic density, hence higher condensable vapor concentrations (e.g., H_2SO_4 and organics). Overall, the nucleation and Aitken mode particles showed distinctly different temporal patterns between the cold and

warm period. The accumulation particles during the warm period showed less consistent patterns, except the obvious impact of aged particles at the mountain site due to the summer prevailing westerly winds (Table 2). Winds from that direction likely inhibited the dispersion of air pollutants in the mountainous region by blocking the outward easterly airflow (Figure 1).

Regardless of the study periods and sites, the average N_{TOT} typically reached a minimum of ~ 1.0×10^4 cm^{-3}in the early morning hours during 03-06 LT, of which could be regarded as the ambient background particle number concentration in the study area. Such background level is consistent with that measured at the roadside in Taiwan (Chen et al., 2010a).

3.5 Size-Fractionated Particle Numbers, Copollutants and Meteorology

The correlation coefficients (r) between the hourly size-fractionated particle numbers, selected copollutants and meteorological parameters at each site are given in Table 5. As the $PM_{2.5}$ correlated very well with the PM_{10} (r = 0.85-0.94), hence the latter is not shown in Table 5. The N_{NUC} at the urban site showed negligible to poor correlations with all the copollutants ($r < 0.11$), weak negative correlation with RH (r = -0.33) and positive correlation with wind speed (WS) (r = 0.17). This indicates that the formation of

nucleation particles at the urban site is not solely related to primary emissions (CO, NO_x and SO_2), and that it is favored under dry and increased wind speed (i.e., daytime hours and enhanced mixing; Figure S1). In downtown Toronto, Canada, Sabaliauskas et al. (2011) however showed the nucleation particles were not correlated with solar radiation and SO_2 but likely better predicted by NO_x. At the coastal and downwind site, the N_{NUC} were positively correlated with SO_2 (r = 0.29 and 0.33, respectively), negatively correlated with RH (r = -0.48 and -0.37, respectively) and positively correlated with WS (r = 0.18 and 0.19, respectively). However, the N_{NUC} at the downwind site was also positively correlated with O_3, indicating that the secondary photochemical processes are possibly an important influential factor. A number of studies have reported NPF events are strongly tied to the photochemistry under the presence of elevated SO_2 (e.g., Verheggen and Mozurkewich, 2002; Stanier et al., 2004a; Young and Keeler, 2007; Wu et al., 2007). Unlike others, the N_{NUC} at the mountain site was moderately correlated with NO_x and CO (r = 0.49 and 0.40, respectively), suggesting a notable connection with primary emissions from local traffic.

The N_{AIT} showed moderate correlations with NO_x and CO (r = 0.46-0.68) at all but the downwind site, where it was more correlated with SO_2 (r = 0.39). This clearly indicates an important connection between the Aitken mode particles and primary

emissions. Earlier studies have shown that the traffic-related particle number emissions are dominated by the UFP fraction, where the mode diameter is highly dependent on the vehicle type and distance to the road (e.g., Zhu et al. 2002; Ogulei et al., 2007; Lonati et al., 2011). At the urban and mountain site, the N_{AIT} were more or less independent of the T, RH and WS ($|r| < 0.15$). At the coastal site, elevated N_{AIT} were related to stagnant (WS; $r = -0.40$), warm (T; $r = 0.28$) and low O_3 ($r = -0.28$) conditions. At the downwind site, elevated N_{AIT} were related to conditions of elevated SO_2 ($r = 0.39$), O_3 ($r = 0.12$), WS ($r = 0.22$) and low RH ($r = -0.27$). This indicates the positive influence of regional transport and photochemistry under dry conditions on the production of Aitken mode particles at the downwind site.

The N_{ACC} at all sites showed moderate to strong positive correlations with all the copollutants SO_2, CO, NO_x and $PM_{2.5}$ ($r = 0.44$-0.86), except that it was not at all correlated with the SO_2 at the mountain site ($r = 0.09$). This suggests that these pollutants share a common source, most likely traffic emissions. The T, RH and WS generally showed weak correlations with the N_{ACC}. Some exceptions include elevated N_{ACC} at the downwind site were moderately related to low temperature, which are indicative of particle buildup in the early evening or nighttime hours (Figure 6). In addition, elevated N_{ACC} at the urban and coastal site were associated with stagnant conditions, suggesting

1 the effects of poor dispersion as well as their local-origin. The strong correlation between
2 the N_{ACC} and $PM_{2.5}$ (r = 0.59-0.86) is in part because a significant fraction of fine particle
3 mass is composed of accumulation particles. For example, Li and Lin (2002) and Lin et al.
4 (2005) have shown that the average $PM_1/PM_{2.5}$ ratio were above 0.76 at urban and traffic
5 sites in Taiwan. Wang et al. (2011a) also observed a strong and stable association between
6 the N_{ACC} and $PM_{2.5}$. In contrast, the N_{NUC} and N_{AIT} showed weak correlations with $PM_{2.5}$
7 ($|r| < 0.25$). This suggests that the UFP and fine particles have different sources or
8 formation processes, particularly the nucleation particles. For example, the correlation
9 between N_{NUC} and $PM_{2.5}$ (r = -0.25) was negative at the mountain site and negligible at
10 the three other sites ($|r| < 0.09$). The former in particular shows that elevated $PM_{2.5}$ could
11 be unfavorable for the production or existence of the nucleation particles. Nevertheless,
12 the Aitken mode and accumulation particles at all of the study sites are predominantly
13 related to primary emissions from traffic. The weak correlations but common traffic-
14 origin between the UFP and accumulation particles underscore that each of the two
15 particle fractions has another source not shared by the other, and/or they have different
16 loss processes in the atmosphere. For example, the secondary photochemical pathway
17 appears to be more relevant to the production of UFP than to that of accumulation
18 particles in the present study area. Furthermore, the much longer atmospheric lifetime of

1 the accumulation particles allows them to survive under polluted environments, in which
2 the UFP are quickly scavenged by pre-existing particles, as illustrated at the mountain site.

3 **4. Conclusion**

4 This study presents first measurements of the submicrometer (10-1000 nm) particle
5 number size distributions at four distinct types of environment (urban, coastal, mountain
6 and downwind) within the Central Taiwan Air Quality Management District during a cold
7 (20.5 °C) and a warm (27.6 °C) period. The urban site showed the highest average
8 submicrometer particle number concentration of up to 3.4×10^4 cm^{-3}, which is 29 to 49%
9 higher than the coastal, mountain and downwind site. The latter three sites showed
10 comparable number concentration, ranging from 1.7×10^4 to 2.2×10^4 cm^{-3}. The average
11 submicrometer particle number concentration at each site showed small variability (<
12 22%) between the cold and warm period, despite notable differences in the
13 meteorological conditions and air quality. During the cold period, the hourly
14 submicrometer particle number concentrations showed distinct diurnal patterns at all but
15 the coastal site with peak concentrations coincided with rush-hour traffic emissions (CO
16 and NO_x). During the warm period, the diurnal patterns across the four sites were more
17 variable and the influence of traffic emissions was relatively weaker. Furthermore, the
18 photochemistry and SO_2 possibly from combustion sources or regional transport were

associated the daytime peak concentrations. Despite having similar submicrometer particle number concentrations, the modal characteristics of the measured particle number size distributions exhibited notable spatial and temporal differences. The ultrafine (10-100 nm) particles and the accumulation (100-1000 nm) particles correlated poorly with each other, even though both were closely connected to traffic emissions. In addition, the accumulation particles were highly correlated with $PM_{2.5}$ and PM_{10}. Such disconnection was likely due to the influences of sources other than road traffic and/or the differences in their ambient loss processes in different environments. Overall, the results indicate modest spatial heterogeneity and strong diurnal variability of the submicrometer particle number concentrations. In addition, there are variable sources or meteorology-dependent formation processes of the ultrafine particles within the study area. In view of the above variability, measurements of the "total" particle number concentrations without discriminating sizes or using PM mass concentrations to estimate particle numbers at a single site would be inadequate for exposure and impact assessment in a region of diverse environments. Instead, at a minimum, the number concentrations of ultrafine and accumulation particles should be measured separately at different types of environment in order to more accurately determine their spatiotemporal variability and hence impact.

Acknowledgments

The authors wish to express their appreciation to the Taiwan EPA for making the air quality monitoring sites available for the present study. The financial support from the Taiwan National Science Council (NSC-97-2218-E-039-002-MY3) and the China Medical University (CMU-96-109) are gratefully acknowledged.

References

Aalto P, Hameri K, Paatero P, Kulmala M, Bellander T, Berglind N, et al. Aerosol particle number concentration measurements in five European cities using TSI-3022 condensation particle counter over a three-year period during health effects of air pollution on susceptible subpopulations. J Air Waste Manage Assoc 2005;55:1064-1076.

Asmi A, Wiedensohler A, Laj P, Fjaeraa A-M, Sellegri K, Birmili W, et al. Number size distributions and seasonality of submicron particles in Europe 2008–2009. Atmos Chem Phys 2011;11:5505-5538.

Bae M-S, Schwab JJ, Hogrefe O, Frank BP, Lala GG, Demerjian KL. Characteristics of size distributions at urban and rural locations in New York. Atmos Chem Phys 2010;10:4521-4535.

1 Baron PA, Willeke K. Aerosol Measurement: Principles, Techniques, and Applications.
2 New York: John Wiley and Sons; 2001.

3 Birmili W, Heinke K, Pitz M, Matschullat J, Wiedensohler A, Cyrys J, Wichmann H-E,
4 Peters A. Particle number size distributions in urban air before and after volatilization.
5 Atmos Chem Phys 2010;10:4643-4660.

6 Bowker GR, Baldauf R, Isakov, V., Khlystov, A., Petersen W. The effects of roadside
7 structures on the transport and dispersion of ultrafine particles from highways, Atmos.
8 Environ., 41, 8128-8139, 2007.

9 Buonanno G, Lall AA, Stabile L. Temporal size distribution and concentration of
10 particles near a major highway. Atmos Environ 2009; 43:1100-1105.

11 Chang S-C, Lee C-T. Secondary aerosol formation through photochemical reactions
12 estimated by using air quality monitoring data in Taipei City from 1994 to 2003.
13 Atmos Environ 2007;41:4002-4017.

14 Chen J-P, Tsai T-S, Liu S-C. Aerosol nucleation spikes in the planetary boundary layer.
15 Atmos Chem Phys 2011;11:7171-7184.

16 Chen S-C, Tsai C-J, Huang C-Y, Chen H-D, Chen S-J, Lin C-C, et al. Chemical mass
17 closure and chemical characteristics of ambient ultrafine particles and other PM

fractions. Aerosol Sci Technol 2010a;44:713-723.

Chen S-C, Tsai C-J, Chou CC-K, Roam G-D, Cheng S-S, Wang Y-N. Ultrafine particles at three different sampling locations in Taiwan. Atmos Environ 2010b;44:533-540.

Cheng W-L. Synoptic weather patterns and their relationship to high ozone concentrations in the Taichung basin. Atmos Environ 2001;35:4971-4994.

Cheng Y-H, Huang C-H, Huang H-L, Tsai C.-J. Concentrations of ultrafine particles at a highway toll collection booth and exposure implications for toll collectors. Sci Total Environ 2010a;409:364-369.

Cheng Y-H, Liu Z-S, Chen C-C. On-road measurements of ultrafine particle concentration profiles and their size distributions inside the longest highway tunnel in Southeast Asia. Atmos Environ 2010b;44:763-772.

Dunn MJ, Jimnez JL, Baumgardner D, Castro T, McMurry PH, Smith JN. Measurements of Mexico City nanoparticle size distributions: observations of new particle formation and growth. Geophy Res Lett 2004;31: doi:10.1029/2004GL019483.

Dusek U, Frank GP, Hildebrandt L, Curtius J, Schneider J, Walter S, et al. Size matters more than chemistry for cloud-nucleating ability of aerosol particles. Science 2006;312:1375-1378.

1 Harrison RM, Jones AM. Multisite study of particle number concentrations in urban air.
2 Environ Sci Technol 2005;39:6063-6070.

3 Heim M, Kasper G, Reischl GP, Gerhart C. Performance of a new commercial electrical
4 mobility spectrometer. Aerosol Sci Technol 2004;38:3-14.

5 Hsieh LY, Kuo SC, Chen CL, Tsai Y.I. Size distributions of nano/micron dicarboxylic
6 acids and inorganic ions in suburban PM episode and non-episodic aerosol. Atmos
7 Environ 2009;43:4396-4406.

8 Hudda N, Cheung K, Moore KF, Sioutas C. Inter-community variability in total particle
9 number concentrations in the eastern Los Angeles air basin. Atmos Chem Phys
10 2010;10:11385-11399.

11 Hussein T, Puustinen A, Aalto PP, Mäkelä JM, Kulmala M. Urban aerosol number size
12 distributions. Atmos Chem Phys 2004;4:391-411.

13 Hussein T, Karppinen A, Kukkonen J, Härkönen J, Aalto PP, Hämeri K, Kerminen VM,
14 Kulmala M. Meteorological dependence of size-fractionated number concentrations of
15 urban aerosol particles. Atmos Environ 2006;40:1427-1440.

16 Jamriska M, Morawska L, Mengersen K. The effect of temperature and relative humidity
17 on size segregated traffic exhaust particle emissions. Atmos Environ 2008;42:2369-

2382.

Jeong CH, Hopke PK, Chalupa DC, Utell MJ. Characteristics of nucleation and growth events of ultrafine particles measured in Rochester, NY. Environ Sci Technol 2004;38:1933-1940.

Kerminen V-M, Lehtinen KJ, Anttila T, Kulmala M. Dynamics of atmospheric nucleation mode particles: a timescale analysis. Tellus B 2004;56:135-146.

Kittelson DB, Watts WF, Johnson JP. Nanoparticle emissions on Minnesota highways. Atmos Environ 2004;38:9-19.

Krudysz MA, Froines JR, Moore KF, Geller MD, Sioutas C. Intra-community spatial variability in particle size distributions in the Los Angeles harbor-area. Atmos Chem Phys 2009;9:1-15.

Kulmala M, Vehkamäki H, Petäjä T, Dal Maso M, Lauri A, Kerminen VM, Birmili W, McMurry PH. Formation and growth rates of ultrafine atmospheric particles: a review of observations. J Aerosol Sci 2004;35:143-176.

Li C-S, Lin C-H. PM1/PM2.5/PM10 characteristics in the urban atmosphere in Taipei. Aerosol Sci Technol 2002;36:469-473.

Lin C-C, Chen S-J, Huang K-L, Hwang W-I, Chang-Chien G-P, Lin W-Y. Characteristics

of metals in nano/ultrafine/fine/coarse particles collected beside a heavily trafficked road. Environ Sci Technol 2005;39:8113-8122.

Lonati G, Crippa M, Gianelle V, Van Dingenen R. Daily patterns of the multi-modal structure of the particle number size distribution in Milan, Italy. Atmos Environ 2011; 45:2434-2442.

McMurry PH, Fink M, Sakurai H, Stolzenburg MR, Mauldin III RL, Smith J, Eisele F, Moore K, Sjostedt S, Tanner D, Huey LG, Nowak JB, Edgerton E, Voisin D. A criterion for new particle formation in the sulfur-rich Atlanta atmosphere. J Geophys Res 2005;doi:10.1029/2005JD005901.

Mejia J, Wraith D, Mengersen K, Morawska L. Trends in size classified particle number concentration in subtropical Brisbane, Australia, based on a five year study. Atmos Environ 2007;41:1064-1079.

Monkkonen P, Koponen I, Lehtinen K, Hameri K, Uma R, Kulmala M. Measurements in a highly polluted Asian Mega City: observations of aerosol number size distribution, modal parameters and nucleation events. Atmos Chem Phys 2005;5: 57-66.

Moore KF, Ning Z, Ntziachristos L, Schauer JJ, Sioutas C. Daily variation in the properties of urban ultrafine aerosol-part I: physical characterization and volatility.

Atmos Environ 2007;41:8633-8646.

Moore KF, Krudysz M, Pakbin P, Hudda N, Sioutas C. Intra-community variability in total particle number concentrations in the San Pedro Harbor area (Los Angeles, California). Aerosol Sci Technol 2009;43:587-603.

Morawska L, Ristovski Z, Jayaratne ER, Keogh DU, Ling X. Ambient nano and ultrafine particles from motor vehicle emissions: characteristics, ambient processing and implications. Atmos Environ 2008;42:8113-8138.

Nel A, Xia T, Mädler L, Li N. Toxic potential of materials at the nanolevel. Science 2006;311:622-627.

Ogulei D, Hopke PK, Ferro AR, Jaques PA. Factor analysis of submicron particle size distributions near a major United States-Canada trade bridge. J Air Waste Manage Assoc 2007;57:190-203.

Paatero P, Aalto P, Picciotto S, Bellander T, Castaño G, Cattani G, et al. Estimating time series of aerosol particle number concentrations in the five HEAPSS cities on the basis of measured air pollution and meteorological variables. Atmos Environ 2005;39:2261-2273.

Pandis SN, Wexler AS, Seinfeld JH. Dynamics of tropospheric aerosols. J Phys Chem

1995;99:9646-9659.

Park K, Park JY, Kwak J-H, Cho GN, Kim J-S. Seasonal and diurnal variations of ultrafine particle concentration in urban Gwangju, Korea: observation of ultrafine particle events. Atmos Environ 2008;42:788-799.

Peng RD, Bell ML, Geyh AS, McDermott A, Zeger SL, Samet JM,et al. Emergency admissions for cardiovascular and respiratory diseases and the chemical composition of fine particle air pollution. Environ Health Perspect 2009;117:957-963.

Reischl GP, Mäkelä JM, Necid J. Performance of the Vienna type differential mobility analyzer at 1.2-20 nm. Aerosol Sci Technol 1997;27:651-672.

Rosenfeld D, Lohmann U, Raga GB, O'Dowd CD, Kulmala M, Fuzzi S, Reissell A, Andreae MO. Flood or drought: how do aerosols affect precipitation? Science 2008;321:1309-1313.

Sabaliauskas KS, Jeong CH, Yao X, Jun YS, Jadidian P, Evans GJ. Five-year roadside measurements of ultrafine particles in a major Canadian city. Atmos Environ 2011; doi:10.1016/j.atmosenv.2011.11.052.

Sardar SB, Fine PM, Yoon H, Sioutas C. Associations between particle number and gaseous co-pollutant concentrations in the Los Angeles Basin. J Air Waste Manage

Assoc 2004;54:992-1005.

Singh M, Phuleria HC, Bowers K, Sioutas C. Seasonal and spatial trends in particle number concentrations and size distributions at the children's health study sites in southern California. J Exposure Anal Environ Epidemiol 2006;16:3-18.

Stanier CO, Khlystov AY, Pandis SN. Nucleation events during the Pittsburgh Air Quality Study: description and relation to key meteorological, gas phase, and aerosol parameters. Aerosol Sci Technol 2004a;38:253-264.

Stanier CO, Khlystov AY, Pandis SN. Ambient aerosol size distributions and number concentrations measured during the Pittsburgh Air Quality Study (PAQS). Atmos Environ 2004b;38:3275-3284.TW EPA. Air Quality Annual Report of R.O.C. (Taiwan) 2009.

US EPA. Particulate Matter Urban-Focused Visibility Assessment. Office of Air Quality Planning and Standards, Research Triangle Park, NC, USA., 2010a.

US EPA. Integrated Science Assessment for Particulate Matter. National Center for Environmental Assessment-RTP division, Office of Research and Development, Research Triangle Park, NC, USA; 2010b.

Verheggen B, Mozurkewich M. Determination of nucleation and growth rates from

observation of SO_2 atmospheric nucleation event. J Geophys Res 2002;107:doi:10.1029/2001JD000683.

Wang F, Ketzel M, Ellermann P, Wåhlin P, Jensen SS, Fang D, et al. Particle number, particle mass and NOx emission factors at a highway and an urban street in Copenhagen. Atmos Chem Phys 2010;10:2745-2764.

Wang Y, Hopke PK, Chalupa DC, Utell MJ. Long-term study of urban ultrafine particles and other pollutants. Atmos Environ 2011a;45:7672-7680.

Wang Y, Hopke PK, Utell MJ. Urban-scale seasonal and spatial variability of ultrafine particle number concentrations. Water Air Soil Pollut 2011b;doi:10.1007/s11270-011-1018-z.

Wehner B, Wiedensohler A. Long term measurements of submicrometer urban aerosols: statistical analysis for correlations with meteorological conditions and trace gases. Atmos Chem Phys 2003;3:867-879.

Westerdahl D, Fruin S, Sax T, Fine P, Sioutas C. Mobile platform measurements of ultrafine particles and associated pollutant concentrations on freeways and residential streets in Los Angeles. Atmos Environ 2005;39: 3597-3610.

Winklmayr W, Reischl GP, Lindner AO, Berner A. A new electro mobility spectrometer

for the measurement of aerosol size distributions in the size range from 1 to 1000 nm. J Aerosol Sci 1990; 22:289-296.

Wu Z, Hu M, Liu S, Wehner B, Bauer S, Ma ßling A, Wiedensohler A, Petäjä T, Dal Maso M, Kulmala M. New particle formation in Beijing, China: statistical analysis of a 1-year data set. J Geophys Res 2007;112:doi:10.1029/2006JD007406.

Yao X, Choi MY, Lau NT, Lau APS, Chan CK, Fang M. Growth and shrinkage of new particles in the atmosphere in Hong Kong. Aerosol Sci Technol 2010;44:639-650.

Young LH, Keeler GJ. Summertime ultrafine particles in urban and industrial air: Aitken and nucleation mode particle events. Aerosol Air Qual Res 2007;7:379-402.

Yu RC, Teh HW, Jaques PA, Sioutas C, Froines JR. Quality control of semi-continuous mobility size-fractionated particle number concentration data. Atmos Environ 2004;38:3341-3348.

Zanobetti A, Schwartz J. The effect of fine and coarse particulate air pollution on mortality: a national analysis. Environ Health Perspect 2009;117:1-40.

Zhang KM, Wexler AS, Zhu YF, Hinds WC, Sioutas C. Evolution of particle number distribution near roadways part II: the road-to-ambient process. Atmos Environ 2004;38:6655-6665.

1 Zhu Y, Hinds WC, Kim S, Sioutas C. Concentration and size distribution of ultrafine
2 particles near a major highway. J Air Waste Manage Assoc 2002;52:1032-1042.

3 Zhu Y, Hinds W, Shen S, Sioutas C. Seasonal trends of concentration and size distribution
4 of ultrafine particles near major highways in Los Angeles. Aerosol Sci Technol
5 2004;38:5-13.

TABLE AND FIGURE CAPTIONS

Table 1. Site and sampling information during the entire study.

Table 2. Hourly averages of meteorological conditions at each site during the two study periods.

Table 3. Hourly averages of air pollutant concentrations at each site during the two study periods.

Table 4. Summary statistics of the hourly size-fractionated number concentrations (10^4 cm^{-3}) at each site during the two study periods.

Table 5. Correlation coefficients between size-fractionated particle number, air pollutant concentrations and meteorological parameters at each site.

Fig. 1. The urban, coastal, mountain and downwind site under study in the Central Taiwan Air Quality Zone.

Fig. 2. The temporal evolution of the measured particle number size distributions at the (a) urban, (b) coastal, (c) mountain and (d) downwind site during the cold and warm period.

Fig. 3. Statistical presentations and ti-modal lognormal fits of the particle number size distributions at the (a) urban, (b) coastal, (c) mountain and (d) downwind site during the cold period.

Fig. 4. Statistical presentations and tri-modal lognormal fits of the particle number size distributions at the (a) urban, (b) coastal, (c) mountain and (d) downwind site during the warm period.

Fig. 5. The diurnal variability of the hourly submicrometer particle number concentrations (N_{TOT}) at each site during the (a) cold and (b) warm period.

Fig. 6. The diurnal variability of the hourly (a) N_{NUC}, (b) N_{AIT} and (c) N_{ACC} at each site during the cold period.

Fig. 7. The diurnal variability of the hourly (a) N_{NUC}, (b) N_{AIT} and (c) N_{ACC} at each site during the warm period.

Table 1. Site and sampling information during the entire study.

Site code	Type	Elev. (m)	Sampling height (m)	Latitude (North)	Longitude (East)	Sampling duration		Aerosol samples[a]
						Cold period	Warm period	
JM	Urban	95	16	24°09'31"	120°39'34"	10/3-10/20/2008, 12/13-12/25/2008	8/9-8/20/2010	8293
SS	Coastal	6	19	24°07'54"	120°28'8"	10/29-11/10/2008, 12/29/'08-1/9/2009	9/15-9/24/2010	6763
PL	Mountain	454	17	23°58'8"	120°58'4"	11/17-11/28/2008, 1/9-1/22/2009	10/11-10/22/2010	5836
JS	Downwind	8	12	23°45'23"	120°40'38"	11/28-12/12/2008	9/2-9/13/2010	5183

a. The time resolution of SMPS measurements was 7-min.

1

2

3

4

Table 2. Hourly averages of meteorological conditions at each site during the two study periods.

Cold period (Oct.-Jan.)	n[a]	T (°C)	RH (%)	WS (m s^{-1})	Prevailing WD	Rain[b] (mm)
Urban	657	22.8	70	0.6	NNE	22.2
Coastal	562	21.5	78	4.3	NNW	33.2
Mountain	436	18.2	70	1.0	WSW	1.6
Downwind	356	17.4	66	0.8	N	0.4
Overall	2011	20.5	71	1.8	NNW	57.4
Warm period (Aug.-Oct.)						
Urban	288	30.3	72	1.1	S	55.6
Coastal	240	27.2	81	2.4	NE	22.2
Mountain	288	25.9	75	1.1	W, WNW	13.0
Downwind[c]	288	26.9	83	1.1	SW, WSW	192.8
Overall	1104	27.6	78	1.4	W	283.6

a. Sample size.

b. Accumulated rain.

c. The downwind site was impacted by a severe tropical storm on September 9 and 10, 2010.

1

2

Table 3. Hourly averages of air pollutant concentrations at each site during the two study periods.

Cold period (20.5 °C)	n	SO_2	CO	O_3	NO_x	$PM_{2.5}$	PM_{10}	$PM_{2.5}/PM_{10}$
Urban	652	3.9	0.7	24.6	34.1	37.9	54.6	69
Coastal	559	4.4	0.3	29.8	15.6	24.6	44.4	55
Mountain	417	3.6	0.5	25.7	20.9	47.7	66.7	72
Downwind	351	2.7	0.5	27.7	22.1	42.8	70.3	61
Overall	1979	3.8	0.5	26.9	23.9	37.2	57.1	65
Warm period (27.6 °C)								
Urban	260	3.2	0.5	24.8	22.4	21.2	31.6	67
Coastal	240	4.2	0.3	27.8	15.4	25.5	44.5	57
Mountain	245	2.2	0.4	34.4	15.0	36.9	49.3	75
Downwind	288	2.2	0.2	25.5	9.2	13.6	23.9	57
Overall	1033	2.9	0.4	28.1	15.4	24.2	37.0	65

Note: CO in ppm, PM in μg m^3, and all others in ppb; $PM_{2.5}/PM_{10}$ in %.

3

4

5

Table 4. Summary statistics of the hourly size-fractionated number concentrations (10^4 cm^{-3}) at each site during the two study periods.

		N_{TOT}		N_{NUC}		N_{AIT}		N_{ACC}		N_{UFP}/N_{TOT}[a]	
Cold period (20.5 °C)	n	Mean	SD	Mean	SD	Mean	SD	Mean	SD	Mean	SD
Urban	641	3.1	1.3	1.1	0.7	1.5	0.7	0.5	0.3	0.81	0.08
Coastal	548	1.7	0.9	0.6	0.5	0.8	0.4	0.3	0.2	0.81	0.10
Mountain	391	1.7	0.8	0.4	0.3	0.8	0.5	0.5	0.2	0.70	0.11
Downwind	331	2.2	1.2	0.5	0.4	1.0	0.6	0.6	0.4	0.69	0.11
Overall	1911	2.2	1.3	0.7	0.6	1.1	0.7	0.5	0.3	0.77	0.11
Warm period (27.6 °C)											
Urban	268	3.4	1.8	1.4	1.2	1.6	0.8	0.4	0.2	0.87	0.08
Coastal	215	2.0	1.3	0.6	0.8	1.0	0.6	0.4	0.3	0.76	0.13
Mountain	260	1.8	0.7	0.4	0.3	0.9	0.4	0.5	0.2	0.70	0.10
Downwind	264	1.7	1.0	0.5	0.4	0.9	0.7	0.3	0.1	0.80	0.10
Overall	1007	2.2	1.4	0.7	0.9	1.1	0.7	0.4	0.2	0.78	0.12

a. The fraction of ultrafine particle (N_{NUC}+N_{AIT}) to total particle (N_{TOT}) number concentration.

Table 5. Correlation coefficients between size-fractionated particle number, air pollutant concentrations and meteorological parameters at each site.

Urban	SO_2	CO	NO_x	O_3	$PM_{2.5}$	T	RH	WS
N_{NUC}	**0.11**	0.08	0.06	0.10	-0.08	0.16	-0.33	0.17
N_{AIT}	0.26	**0.62**	0.54	-0.05	0.20	0.14	-0.11	-0.08
N_{ACC}	0.45	**0.77**	0.73	-0.04	0.72	0.15	0.03	-0.31
Coastal								
N_{NUC}	**0.29**	0.07	0.10	-0.01	-0.05	-0.15	-0.48	0.18
N_{AIT}	0.44	0.46	**0.58**	-0.28	0.19	0.29	0.01	-0.40
N_{ACC}	0.53	0.62	0.57	-0.26	**0.78**	0.12	0.03	-0.39
Mountain								
N_{NUC}	0.09	0.40	**0.49**	-0.01	-0.25	0.15	-0.06	-0.02
N_{AIT}	0.13	0.57	**0.68**	0.04	-0.05	0.15	0.05	-0.09
N_{ACC}	0.01	**0.62**	0.49	0.11	0.59	0.14	0.13	-0.14
Downwind								
N_{NUC}	**0.33**	0.21	0.17	0.28	0.09	0.12	-0.37	0.19
N_{AIT}	**0.39**	0.29	0.26	0.32	0.25	0.16	-0.27	0.22
N_{ACC}	0.44	0.66	0.62	0.12	**0.86**	-0.42	-0.27	-0.12

Bold numbers are the highest correlation coefficients between each particle size fraction and copollutants.

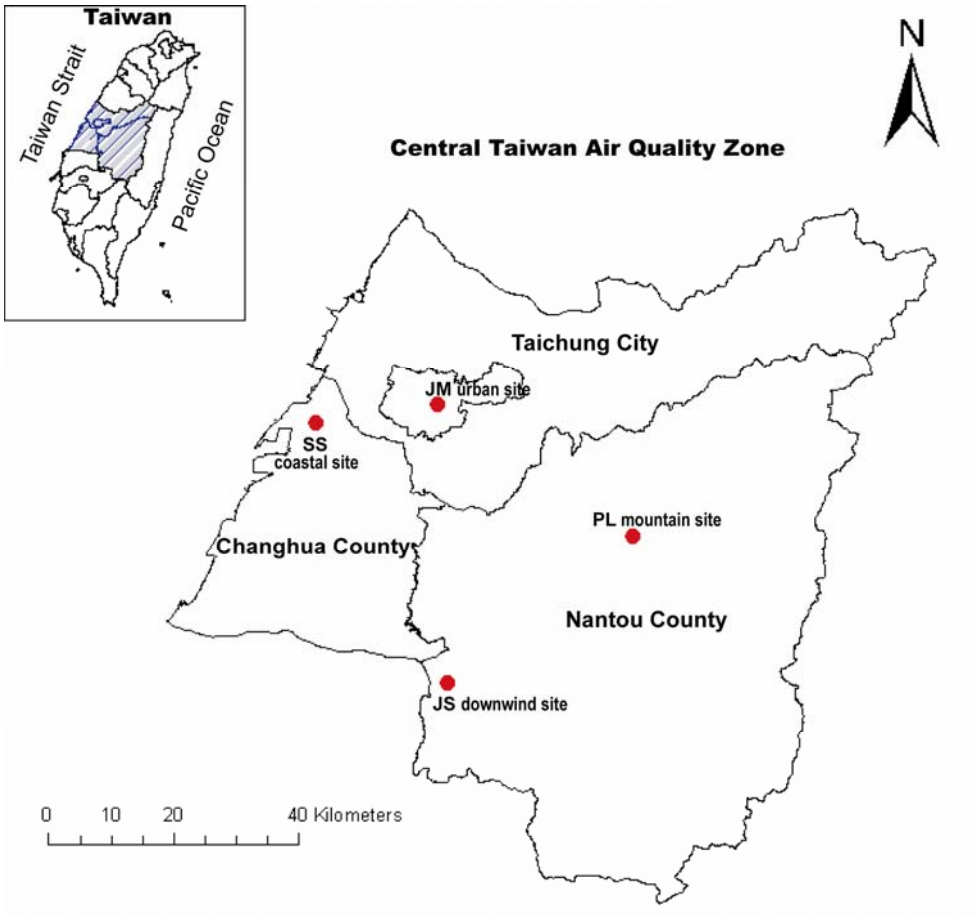

Fig. 1. The urban, coastal, mountain and downwind site under study in the Central Taiwan Air Quality Zone.

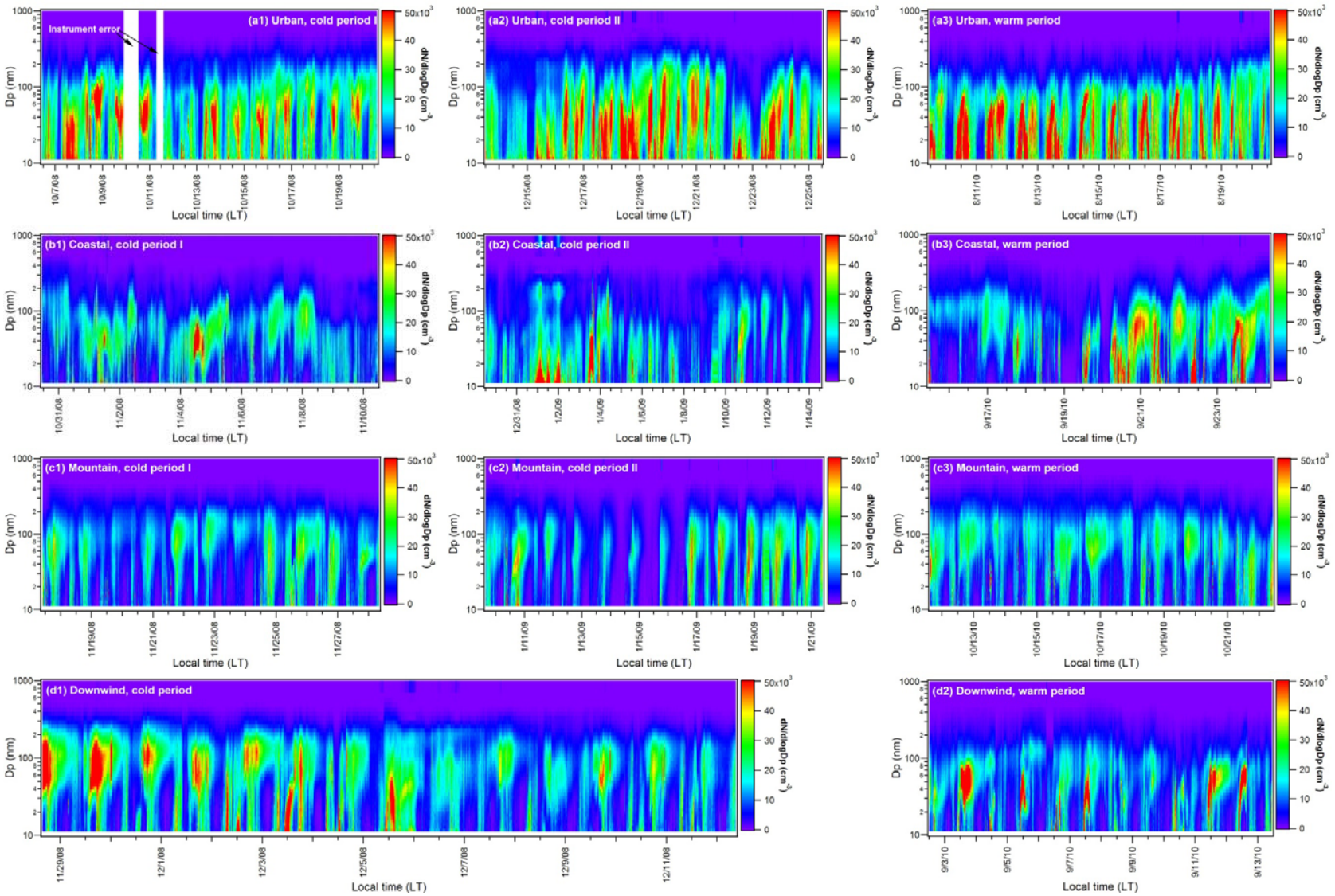

Fig. 2. The temporal evolution of the measured particle number size distributions at the (a) urban, (b) coastal, (c) mountain and (d) downwind site during the cold and warm period.

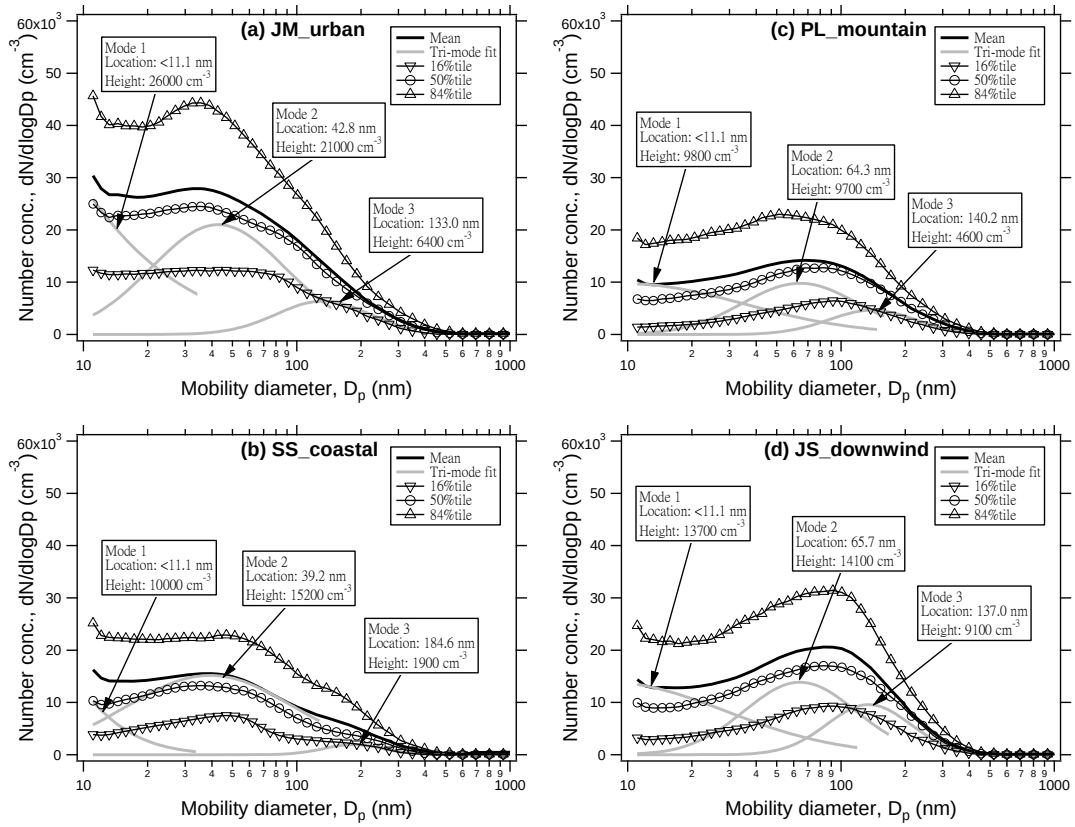

Fig. 3. Statistical presentations and tri-modal lognormal fits of the particle number size distributions at the (a) urban, (b) coastal, (c) mountain and (d) downwind site during the cold period.

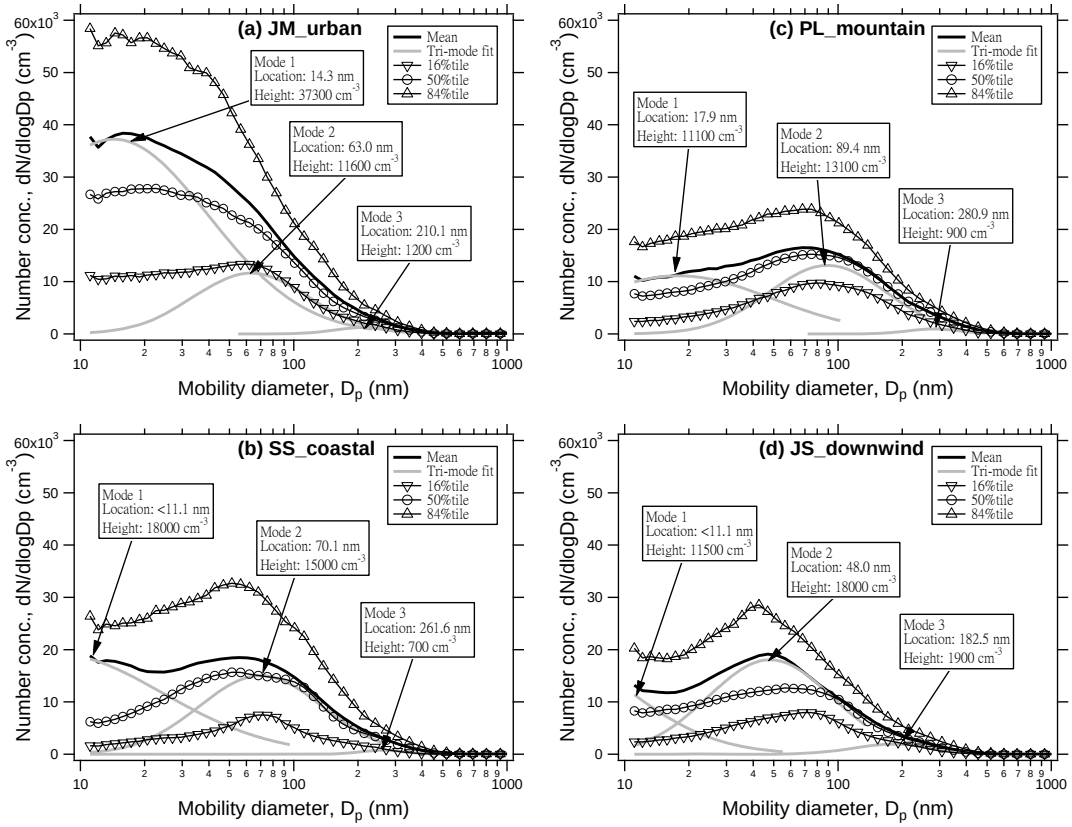

Fig. 4. Statistical presentations and tri-modal lognormal fits of the particle number size distributions at the (a) urban, (b) coastal, (c) mountain and (d) downwind site during the warm period.

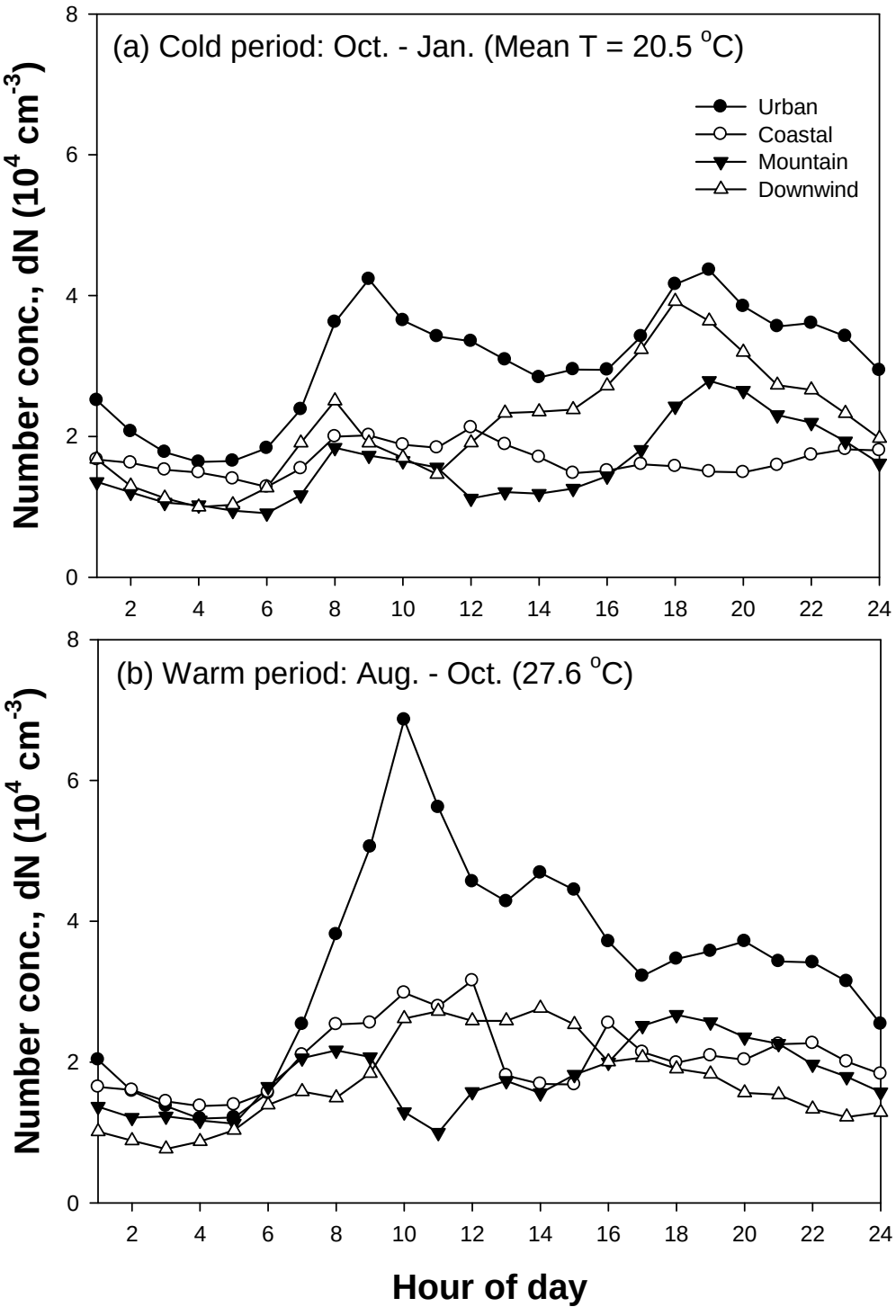

Fig. 5. The diurnal variability of the hourly submicrometer particle number concentrations (N_{TOT}) at each site during the (a) cold and (b) warm period.

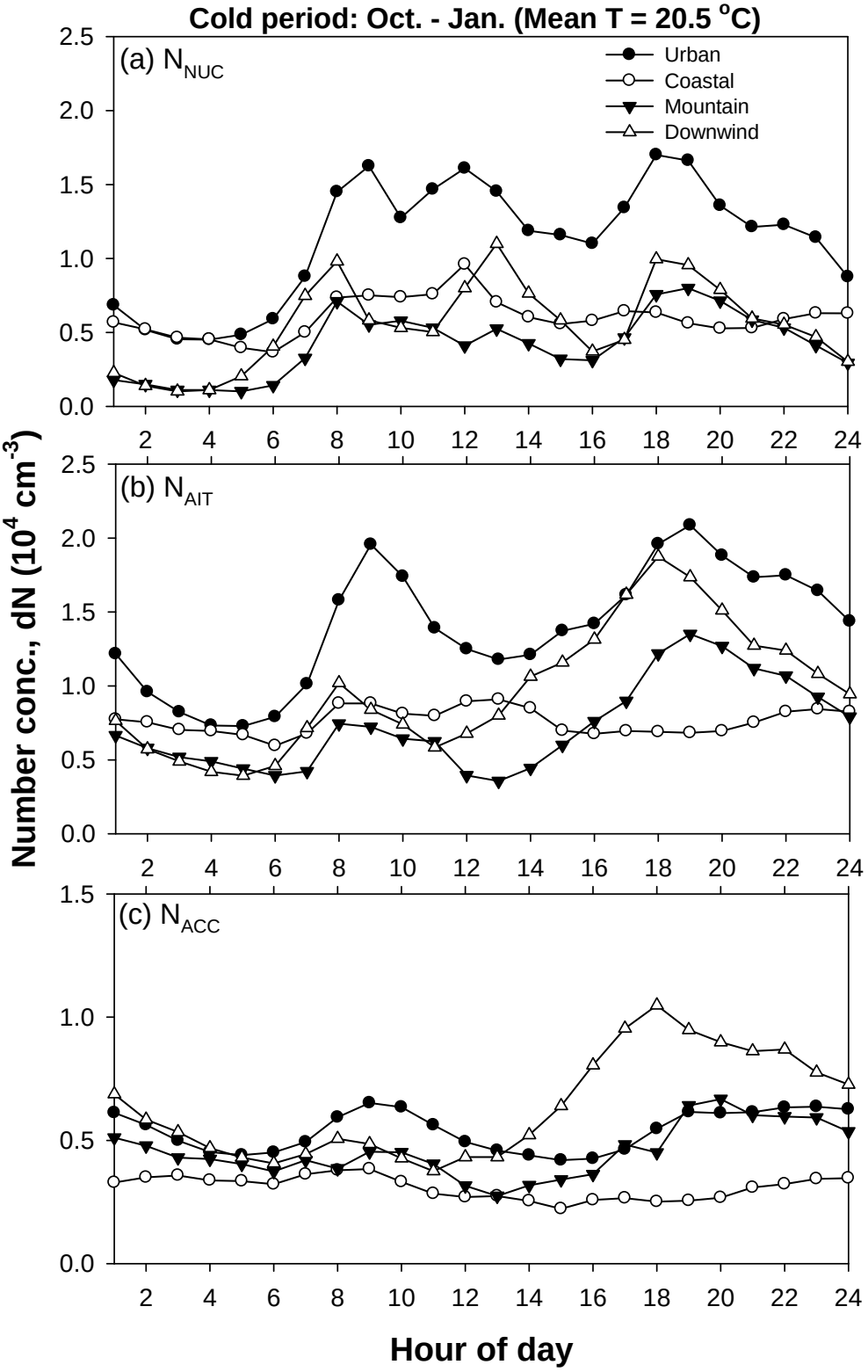

Fig. 6. The diurnal variability of the hourly (a) N_{NUC}, (b) N_{AIT} and (c) N_{ACC} at each site during the cold period.

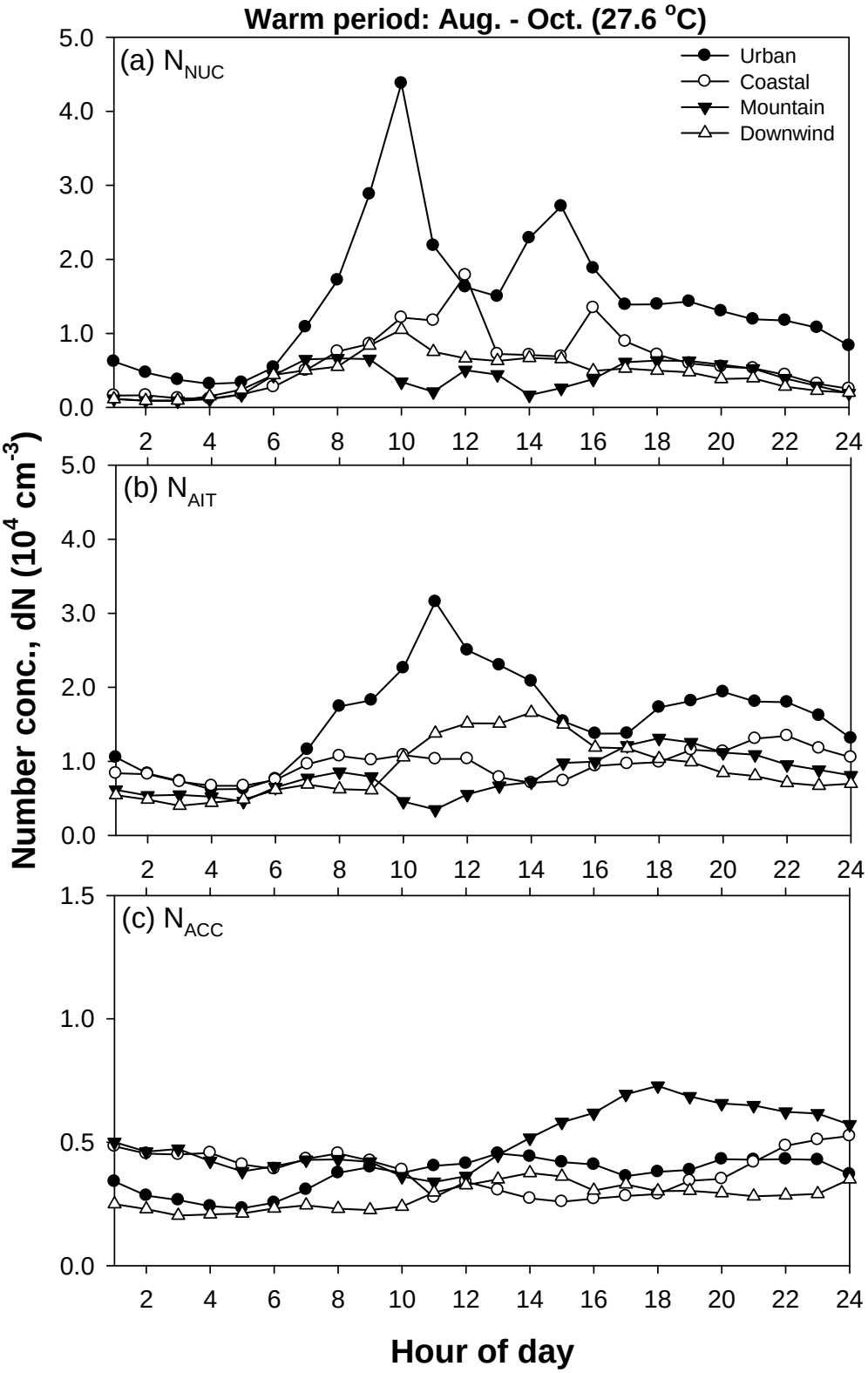

Fig. 7. The diurnal variability of the hourly (a) N_{NUC}, (b) N_{AIT} and (c) N_{ACC} at each site during the warm period.

SUPPLEMENTAL MATERIAL

Spatiotemporal variability of submicrometer particle number size distributions in an air quality management district

Li-Hao Young[a,*], Yi-Ting Wang[a], Hung-Chieh Hsu[a], Ching-Hui Lin[a], Yi-Jyun Liou[a], Ying-Chung Lai[a], Yun-Hua Lin[a], Wei-Lun Chang[a], Hung-Lung Chiang[b], Man-Ting Cheng[c]

[a] Department of Occupational Safety and Health, China Medical University, 91, Hsueh-Shih Road, Taichung 40402, Taiwan

[b] Department of Health Risk Management, China Medical University, 91, Hsueh-Shih Road, Taichung 40402, Taiwan

[c] Department of Environmental Engineering, National Chung Hsing University, 250, Kuo-Kuang Road, Taichung 40254, Taiwan

*Corresponding author: Tel.: +886-4-2205-3366 Ext.6219; Fax.: +886-4-2207-5711; Email: lhy@mail.cmu.edu.tw

TABLE AND FIGURE CAPTIONS

Table S1. Averages of daily mean total submicrometer number concentrations (N_{TOT}, 10^4 cm^{-3}) on weekdays and weekends during the two study periods.

Fig. S1. The site-specific diurnal variability of wind speed during the (a) cold and (b) warm period.

Fig. S2a. The site-specific diurnal variability of air pollutants during the cold period.

Fig. S2b. The site-specific diurnal variability of air pollutants during the warm period.

Table S1. Summary statistics of daily mean total submicrometer number concentrations (N_{TOT}, 10^4 cm^{-3}) on weekdays and weekends during the two study periods.

	Weekday N_{TOT}			Weekend N_{TOT}		
Period	n	Average	SD	n	Average	SD
Cold	67	2.3	0.9	24	2.3	1.2
Warm	36	2.3	0.8	10	1.9	0.8
Overall	103	2.3	0.9	34	2.2	1.1

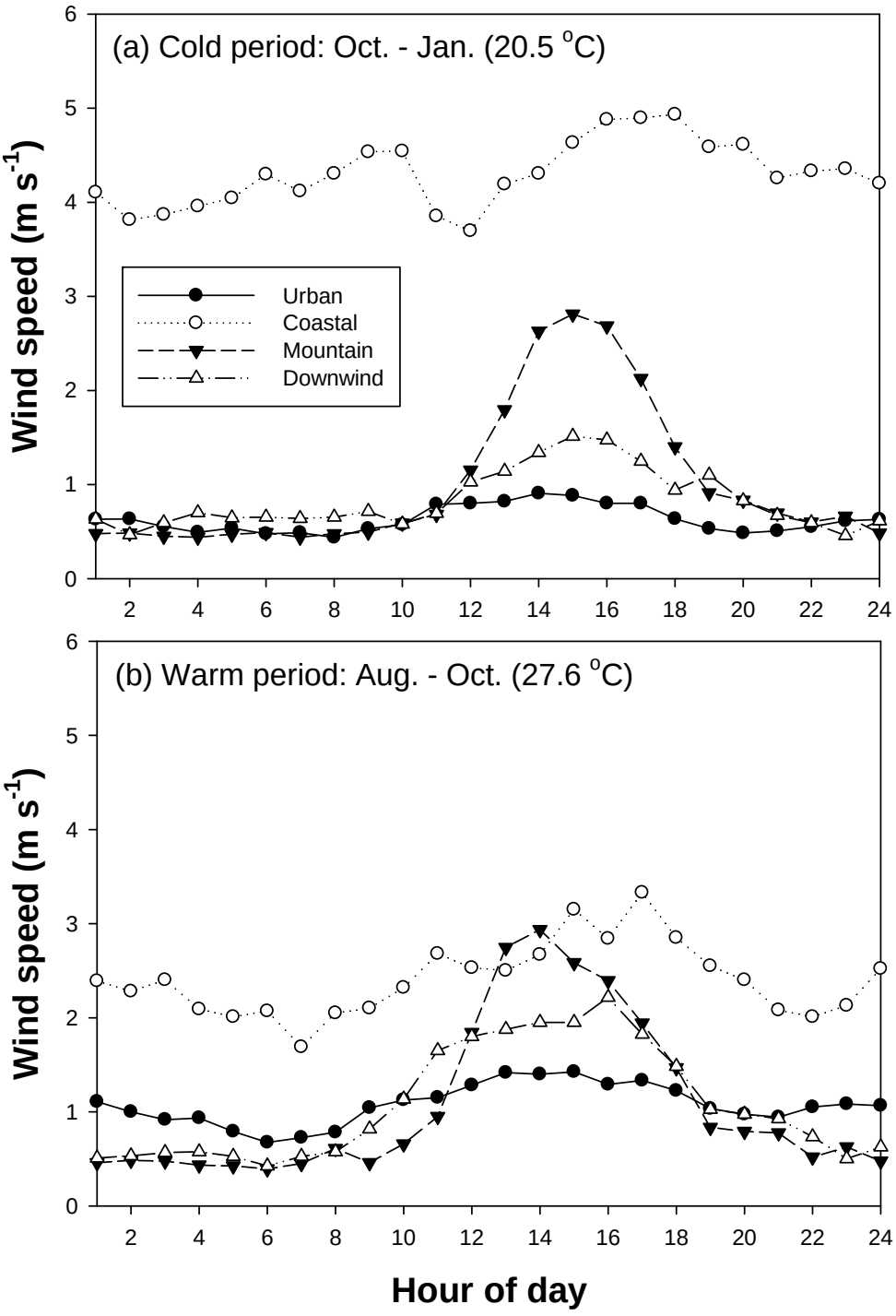

Fig. S1. The site-specific diurnal variability of wind speed during the (a) cold and (b) warm period.

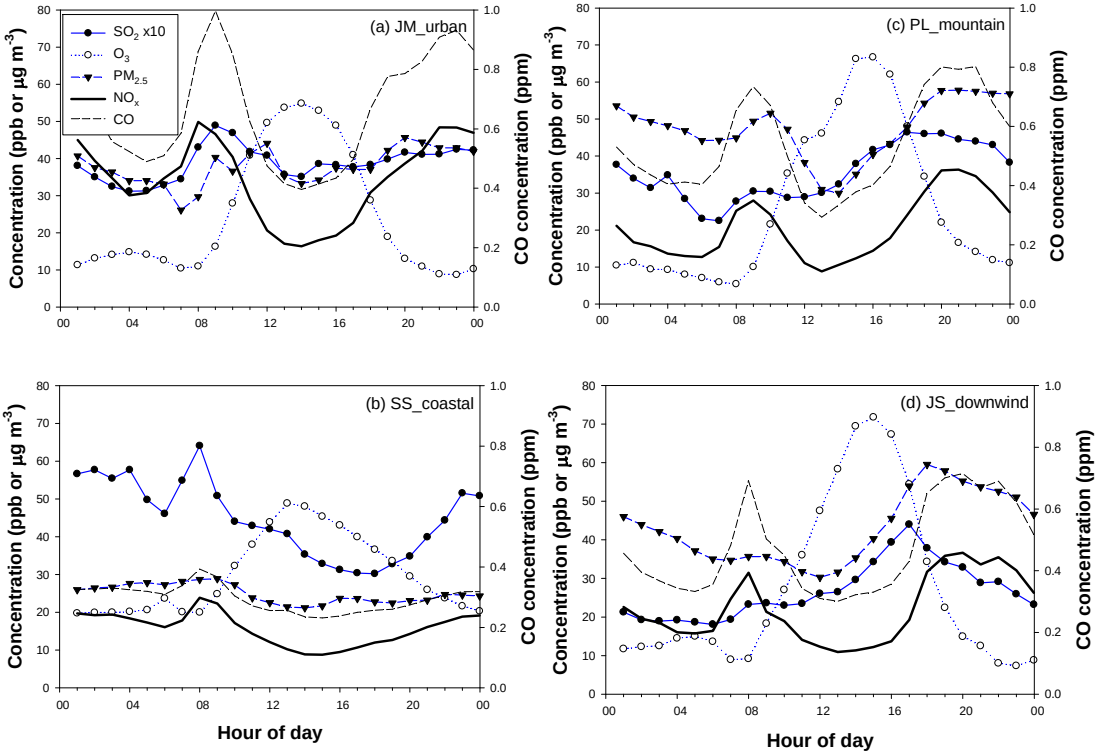

Fig. S2a. The site-specific diurnal variability of air pollutants during the cold period.

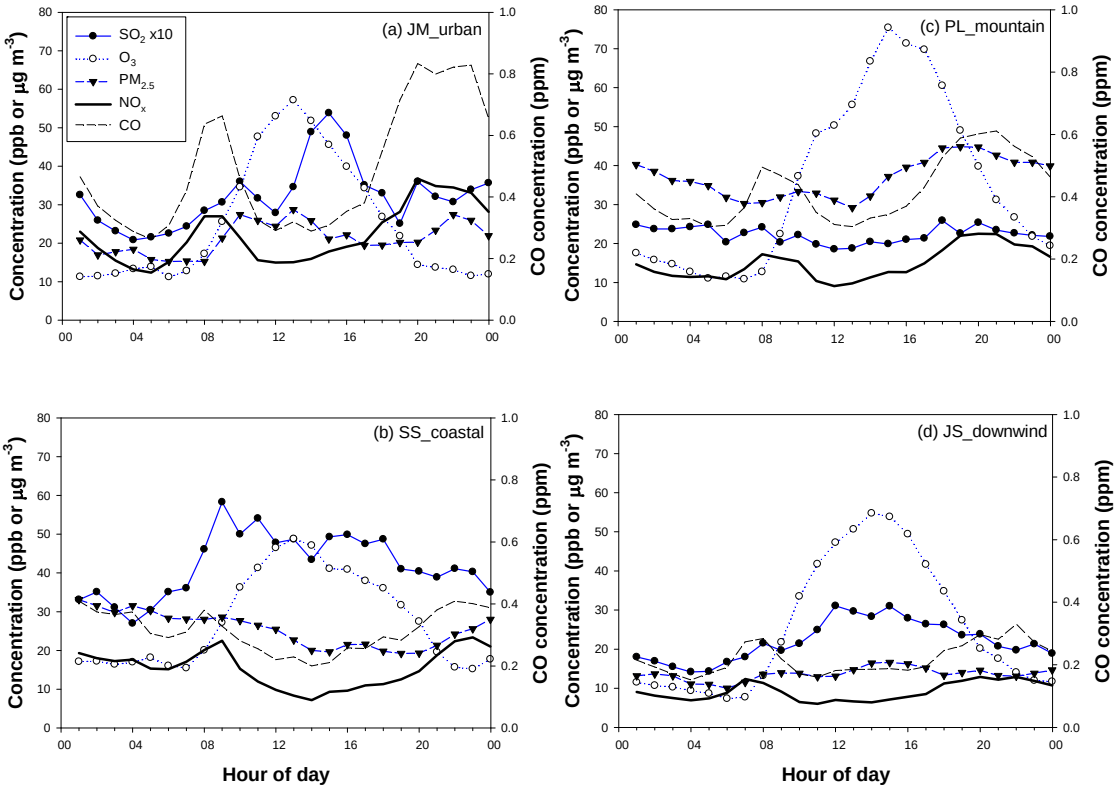

Fig. S2b. The site-specific diurnal variability of air pollutants during the warm period.